AIP Advances

# Capsule-like voids in SiC single crystal: Phase contrast imaging and computer simulations

V. G. Kohn, T. S. Argunova, and J. H. Je

Citation: AIP Advances **4**, 097134 (2014); doi: 10.1063/1.4896512
View online: http://dx.doi.org/10.1063/1.4896512
View Table of Contents: http://scitation.aip.org/content/aip/journal/adva/4/9?ver=pdfcov
Published by the AIP Publishing

**Articles you may be interested in**

Spatial Coherence Preservation By Synthetic Single Diamond Crystals
AIP Conf. Proc. **705**, 736 (2004); 10.1063/1.1757901

Phase field microelasticity theory and simulation of multiple voids and cracks in single crystals and polycrystals under applied stress
J. Appl. Phys. **91**, 6435 (2002); 10.1063/1.1471389

Formation mechanism of interfacial voids in the growth of SiC films on Si substrates
J. Vac. Sci. Technol. A **19**, 2636 (2001); 10.1116/1.1399321

Hexagonal voids and the formation of micropipes during SiC sublimation growth
J. Appl. Phys. **89**, 4625 (2001); 10.1063/1.1355716

Role of oxygen in the formation of voids at the SiC–Si interface
Appl. Phys. Lett. **70**, 1533 (1997); 10.1063/1.118609


All article content, except where otherwise noted, is licensed under a Creative Commons Attribution 3.0 Unported license. See: http://creativecommons.org/licenses/by/3.0/
Downloaded to IP: 37.144.188.193 On: Wed, 24 Sep 2014 11:09:02

AIP ADVANCES **4**, 097134 (2014)

# Capsule-like voids in SiC single crystal: Phase contrast imaging and computer simulations

V. G. Kohn,[1] T. S. Argunova,[2] and J. H. Je[3,a]
[1]*National Research Center "Kurchatov Institute", 123182, Moscow, Russia*
[2]*Ioffe Physical-Technical Institute, RAS, 194021 St. Petersburg, Russia*
[3]*X-ray Imaging Center, Department of Materials Science and Engineering, Pohang University of Science and Technology, San 31 Hyoja-dong, Namku, 790-784 Pohang, Republic of Korea*

(Received 17 June 2014; accepted 15 September 2014; published online 23 September 2014)

The results of observation of capsule-like voids in silicon carbide (6*H*-SiC) single crystal by means of a phase contrast imaging technique with synchrotron radiation at the Pohang Light Source as well as computer simulations of such images are presented. A pink beam and a monochromated beam were used. The latter gives more pronounced images but they still are smoothed due to a finite detector resolution and the spatial coherence of the beam. Sizes and a structure of far field images are different from these of the objects. The computer simulations allow us to reproduce a shape and a size of the capsule-like void. © *2014 Author(s). All article content, except where otherwise noted, is licensed under a Creative Commons Attribution 3.0 Unported License.* [http://dx.doi.org/10.1063/1.4896512]

## I. INTRODUCTION

Silicon carbide (SiC) single crystals are hard and heat resistant materials. They have high thermal conductivity, high electric field breakdown strength, high maximum current density, and very low coefficient of thermal expansion. This is why they are more promising than silicon for high-power devices. Significant advancements in the growth of SiC by sublimation technique (see, e.g., reviews[1,2]) have stimulated mass production of large diameter and good quality boules. However, most SiC wafers still contain imperfections which can be correlated with degradation of SiC based devices, and voids of various shapes and origins are particularly damaging.

Micropipes are known to nucleate at second phase inclusions,[3] foreign polytype boundaries,[4] cavities,[5,6] *etc.* in the shape of a cylinder with circular or elliptic cross section. X-ray topography[1,3,5] and phase contrast imaging[7–15] allows one to observe them non-destructively inside the crystal bulk.

The phase contrast technique provides information due to a phase shift in an x-ray coherent wave. It is widely used in materials research for high resolution imaging.[16–19] In detecting micropipes it has some difficulties because the phase shift created by a micropipe is small, and the size of elliptic cross section is comparable with the detector resolution (about one micron). The image contrast is very weak and the image is of small size when detected at a small distance from a crystalline sample, i.e. in the near field. To overcome these problems we registered images at rather large distances, i.e. in the far field, using a pink synchrotron radiation (SR) beam. In this article the term "pink SR beam" is used for the radiation from a bending magnet without a monochromator.

Under the far field conditions an image has a larger size compared to a small object, but a different structure. Therefore an inverse problem solution is necessary. The pink beam provides a large number of photons which are necessary for the registration of signal with a low statistical noise. Despite the absence of a monochromator the pink beam exists naturally because the

[a]Electronic mail: jhje@postech.ac.kr

 © Author(s) 2014

All article content, except where otherwise noted, is licensed under a Creative Commons Attribution 3.0 Unported license. See: http://creativecommons.org/licenses/by/3.0/
Downloaded to IP: 37.144.188.193 On: Wed, 24 Sep 2014 11:09:02

intensity of high photon energies decrease, while the photons of low energies are absorbed in a thick (490 $\mu$m) crystalline sample.

For the solution of the inverse problem we elaborated a special computer program. The program simulated phase contrast images of micropipe for various photon energies and summed them according to the synchrotron radiation effective spectrum to one pink beam image (see[15] and references therein). Such an image depends on the two elliptic cross section diameters of the object. They were varied to find the diameters which fitted experimental phase contrast profiles to calculated ones. It was shown that for the micropipes with very small cross sections the two diameters could not be reproduced, and only the cross section area could be obtained with a good accuracy.[11,12]

In this work we report on capsule-like voids that are for the first time observed. The voids are of different kind from the objects investigated in our previous works. Such a void looks like a cylinder with a circular cross section and a finite length ended in hemispheres. In addition, we perform 2D calculation for simulating the images of the voids, which is different from 1D calculation for micropipes.[7–15]

We note that voids of various shapes and sizes can be observed in SiC crystals by the phase contrast technique. However, the capsule-like voids have a simple shape, a small size, and their origin is of interest from the point of view of initial void formation. In this work SiC crystals were grown on "*a*-plane" [i.e., $(11\bar{2}0)$ plane] seeds when dislocated micropipes were not formed.[20] However, other voids formed into the crystal volume, grew, obtained faceted shapes characteristic of the crystal habit, or dissolved. Capsule-like voids could move in the direction determined by a temperature gradient and coagulate into tubular voids.

It seems to us that a capsule-like void grows due to motion of vacancies to a void. They can come inside the void but can not go outside due to elastic forces. Under isotropic conditions the void shape is spherical. Under the conditions, where the crystal has some direction of fast vacancy movement, the sphere is transformed to the capsule-like object.

We demonstrate the peculiarities of the phase contrast images of such voids by means of computer simulations on the base of the theory of x-ray phase contrast. We obtain the parameters of the capsule-like void from a comparison of the experimental images with the simulated ones.

## II. EXPERIMENT

The samples were prepared from a 6*H*-SiC boule produced by means of *a*-face growth using profiled seeds. To obtain crystals free from micropipes Ohtani *et al.*[20] reported that the growth on the $(11\bar{2}0)$ surfaces was effective resulting in a reduced stacking fault density. However, a large density of dislocations can remain within the crystal. To reduce dislocations threading from the seed the growth on mesa structures can be used. Lateral growth on the sides of mesas was accompanied by a decrease in the density of threading dislocations.[21,22] Each of these procedures to prevent the propagation of micropipes or dislocations has been used by others,[20–22] but here they are combined in one procedure.

First, a 6*H*-SiC ingot was grown on the (0001) face of a SiC seed by a sublimation sandwich method[23] at the growth temperature 2100-2200°C with the growth rate of 0.5 mm $\cdot$ h$^{-1}$ and sliced into $(11\bar{2}0)$ wafers. Micropipe and dislocation densities were 20 cm$^{-2}$ and $10^4$ cm$^{-2}$, respectively. In the second step, these wafers were used as *a*-plane seeds for further growth in the $[11\bar{2}0]$ direction. A groove network 50 $\mu$m wide, 50 $\mu$m deep and having a spacing of 500 $\mu$m was made by a diamond saw on the surface of each seed, and the seed surfaces were etched.

Mokhov *et al.*[22] reported studies of the structural quality of the crystals grown on (0001) mesa surfaces. In this case, KOH-defect selective etching analysis of the wafers cut perpendicular to the [0001] growth direction showed that there were no etching features in the regions above the flattened grooves. The density of etching features in the central regions of flat mesas were nearly equal to those of the seeds. The authors proposed that dislocations and micropipes propagated into the grown crystal from the seed rather than generated during growth, because neither the lateral growth from the mesa sidewalls nor the layer-by-layer growth on the flat mesas could lead to these defects formation.

All article content, except where otherwise noted, is licensed under a Creative Commons Attribution 3.0 Unported license. See: http://creativecommons.org/licenses/by/3.0/
Downloaded to IP: 37.144.188.193 On: Wed, 24 Sep 2014 11:09:02

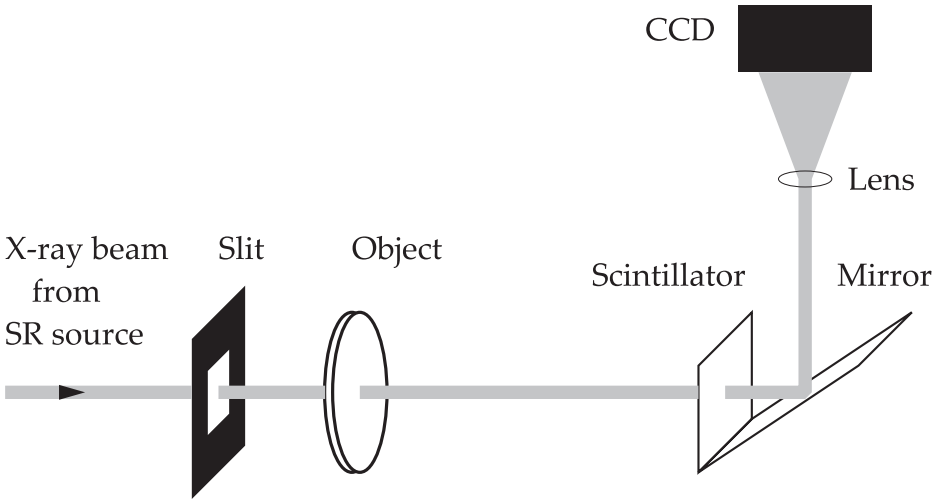


FIG. 1. Schematic of experiment. See text for details.

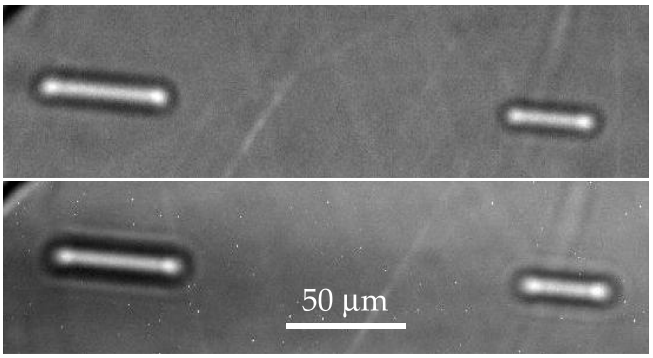


FIG. 2. The images of two capsule-like voids. Top panel: polychromatic radiation. Bottom panel: monochromatic (16 keV) radiation.

In the present work the growth on $(11\bar{2}0)$ mesa substrates was performed with the purpose to control dislocation density.

The conditions for the *a*-plane growth were almost the same as above described. The Argon pressure in the growth chamber was $1 \cdot 10^{-3}$–$7 \cdot 10^{-3}$ MPa. The grown crystal was sliced along the growth direction into (0001) wafers mechanically and chemically polished on both sides. Residual damage on the sample surface contributes to the image and should be removed.

The wafers were investigated by the phase contrast imaging technique using the 6D X-ray micro-imaging beamline at the Pohang Light Source. The beam source with a size 160 $\mu$m × 60 $\mu$m (H × V) from a bending magnet was located 34 m from a sample. The experimental setup is shown in Fig. 1. Behind the sample, the radiation is converted into visible light by a $CdWO_4$ crystal-scintillator (150–200 $\mu$m thick). The visible light is reflected from a polished silicon mirror with the aim to reach CCD camera. The light image is magnified by a lens. The CCD matrix of pco.4000 camera (supplied with a thermo-electrical Peltier cooler) had 4008 (H) × 2672 (V) pixels size, one pixel being of 9 $\mu$m (H) × 9 $\mu$m (V). Using a 20× lens the effective pixel size was 0.45 $\mu$m, and the view field was 1804 × 1202 $\mu m^2$.

Polychromatic (pink) beam as well as a high-flux monochromatic beam (made with a multilayer monochromator) were utilized. In the case of a pink beam the energy spectrum, shown in Figure 2 of our previous article,[15] had a maximum intensity at 16 keV and FWHM as 11 keV. The temporal coherence length was $L_{tc}^{p} = 1.2$ Angstroms.[15] It increased to $L_{tc}^{m}$=194 Angstroms in the case of the multilayer ($\Delta E/E = 0.4\%$ Mo/$B_4C$) tuned to the energy $E = 16$ keV.

All article content, except where otherwise noted, is licensed under a Creative Commons Attribution 3.0 Unported license. See: http://creativecommons.org/licenses/by/3.0/
Downloaded to IP: 37.144.188.193 On: Wed, 24 Sep 2014 11:09:02

All studied wafers contained sparse voids which could be classified into micro, meso and macro scale categories. The micro scale category included the biggest population of spherical and capsule-like voids. The meso scale voids looked tubular with smooth walls, and the macro-voids obtained asymmetric hexagonal shapes.

Figure 2 shows the parts of two images recorded from one fragment of the SiC wafer with the pink (the top panel) and the monochromated (the bottom panel) beams. The sample-to-detector distance is 35 cm. The sample thickness is 50 $\mu$m. One can see that the monochromated beam allows us to obtain a more pronounced picture. However, exposure times were 25 ms and 190 s for the pink and the monochromated beams, respectively.

## III. COMPUTER SIMULATIONS

An algorithm for a computer simulation of x-ray phase contrast images was described many times since the work.[24] The sources of coherent synchrotron radiation are separate electrons inside the storage ring which radiate the narrow beam. The total radiation inside the beam at long distance $z_0$ from the source, i.e. in front of a sample, can be split into monochromated harmonics (see, for example,[25] for details) which can be approximated by

$$E(x, y, z_0) = \exp(iKz_0)P_2(x, y, z_0) \tag{1}$$

where $K = \omega/c = 2\pi/\lambda$, $\omega$ is the frequency of radiation, $c$ is the speed of light, $\lambda$ is the wavelength, and

$$P_2(x, y, z) = P(x, z)P(y, z), \quad P(x, z) = \frac{1}{(i\lambda z)^{1/2}} \exp\left(i\pi \frac{x^2}{\lambda z}\right). \tag{2}$$

Here we use a Cartezian coordinate system with the $z$-axis along the beam (optical axis) and the $x$, $y$ axes along the horizontal and vertical axes in the plane normal to the beam.

The formulae (1) and (2) correspond to the paraxial approximation which is valid for the x-ray radiation with a good accuracy. The object can be described by a transmission function. We note that the phase factor $\exp(iKz)$ can be omitted because it does not influence the intensity which is only registered by a detector. Our object is a void inside the crystal in the form of a plate. The crystal itself does not influence the intensity distribution and causes only a homogeneous decrease in the intensity due to absorption.

We denote as $t_0$ a maximum thickness of the void and consider a part of the crystal plate of this thickness. The void influences the radiation field by increasing the phase and the amplitude of the wave as compared with the part of the crystal without the void. This phenomenon can be taken into account by the factor

$$T(x, y) = \exp(iK[\delta - i\beta]t(x, y)) \tag{3}$$

where $\delta$ and $\beta$ are the refraction and absorption parameters so that the complex index of refraction of the material is $n = 1 - \delta + i\beta$, and $t(x, y)$ is a variable thickness of the void along the optical axis. A usage of (3) is convenient for the calculation because $T(x, y)$ equals unity outside the void. After the calculation we need to multiply the intensity by a factor $\exp(-\mu_0 t_0)$ to take into account the absorption inside the slab. Here $\mu_0 = 2K\beta$ is a linear absorption coefficient.

The wave field at the distance $z_1$ behind the crystal can be calculated within the Kirchhoff integral relation as a convolution

$$E(x, y, z_t) = \int dx_1 dy_1 P_2(x - x_1, y - y_1, z_1)T(x_1, y_1)P_2(x_1, y_1, z_0) \tag{4}$$

where $z_t = z_0 + z_1$. This integral can be transformed to the equivalent form which is more convenient for a calculation,

$$E(x, y, z_t) = P_2(x, y, z_t) \int dx_1 dy_1 P_2(x_r - x_1, y_r - y_1, z_r)T(x_1, y_1), \tag{5}$$

All article content, except where otherwise noted, is licensed under a Creative Commons Attribution 3.0 Unported license. See: http://creativecommons.org/licenses/by/3.0/
Downloaded to IP: 37.144.188.193 On: Wed, 24 Sep 2014 11:09:02

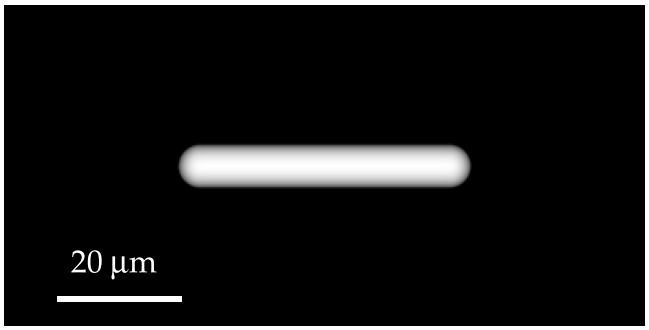


FIG. 3. A gray map of the function $t(x, y)$, the black color for $t = 0$, the white color for $t = t_0 = 7\ \mu$m.

where $x_r = xz_0/z_t$, $y_r = yz_0/z_t$, $z_r = z_1z_0/z_t$. It is convenient to consider a relative wave field

$$A(x, y, z_t) = \frac{E(x, y, z_t)}{P_2(x, y, z_t)} \tag{6}$$

and to transform the expression to the integral of finite limits

$$A(x, y, z_t) = 1 + \int dx_1 dy_1 P_2(x_r - x_1, y_r - y_1, z_r)[T(x_1, y_1) - 1]. \tag{7}$$

Finally we have the expression for the phase contrast, which is registered by a detector, as follows

$$C(x, y) = |A(x, y, z_t)|^2 \exp(-\mu_0 t_0) \tag{8}$$

For the capsule-like void with a cylindrical cross section we use the formula for $t(x, y)$,

$$t(x, y) = t_0 \left(d - \frac{y^2}{R}\right)^{1/2} \tag{9}$$

where $t_0 = 2R$, and

$$\begin{array}{cc} d = 1 & -a < x < a \\ d = 1 - (x + a)^2/R^2 & x < -a \\ d = 1 - (x - a)^2/R^2 & x > a \end{array} \tag{10}$$

In this case we have only two parameters: the curvature radius $R$ and the length of the region having a constant cross section $2a$. The calculation of the convolution (7) was performed by means of two Fourier transformations. First, we calculate the Fourier image of $[T - 1]$, then multiply it by the Fourier image of $P_2(x, y, z_r)$ and then calculate the reverse Fourier image. The procedure of FFT (fast Fourier transformation) was performed on the set of 2048*1024 points with the step of 0.05 $\mu$m.

## IV. DISCUSSION AND CONCLUSIONS

We have performed simulations of phase contrast images for the parameters of the experiment, i.e. $z_0 = 34$ m, $z_1 = 35$ cm, energy $E = 16$ keV, $a = 20\ \mu$m and various values of $R$ with the aim to obtain the same image as shown in Figure 2. We have found that $R = 3.5\ \mu$m is the value which provides the best fit. The function $t(x, y)$ within the calculation area is shown in Figure 3. We use the gray scale with the black color for $t = 0$ and the white color for $t = t_0 = 7\ \mu$m.

The calculated phase contrast image for a point source (fully coherent) is shown in the top panel of Figure 4. To show the contrast perfectly we use the black color for a minimum relative intensity 0.26 and the white color for a maximum 3.47. One can see that the image does not coincide with the $t(x, y)$ distribution, which is proportional to the phase shift map. The reason is that the size of void is

All article content, except where otherwise noted, is licensed under a Creative Commons Attribution 3.0 Unported license. See: http://creativecommons.org/licenses/by/3.0/
Downloaded to IP: 37.144.188.193 On: Wed, 24 Sep 2014 11:09:02

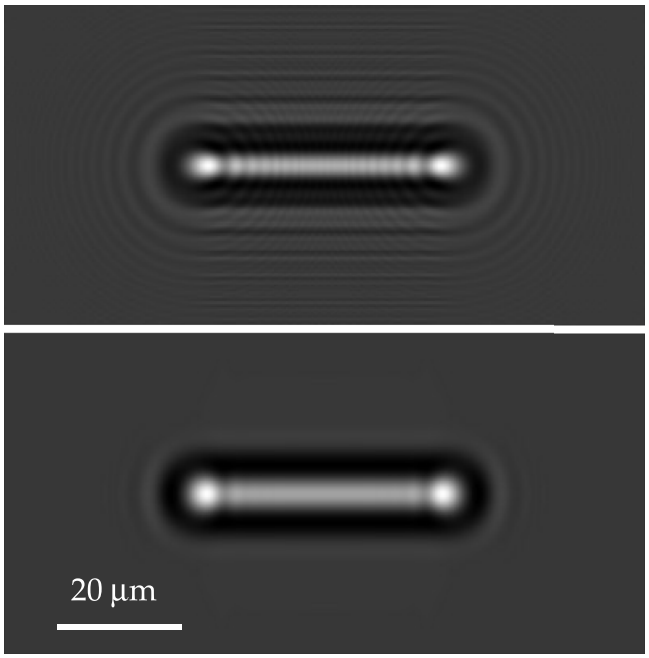


FIG. 4. The calculated image (phase contrast) of a capsule-like void. Top panel: point source and ideal detector resolution, the black color corresponds to 0.26, the white color is for 3.47. Bottom panel: a smoothed image after a calculation of convolution with a Gaussian having FWHM 2 $\mu$m vertically and 4 $\mu$m horizontally.

not very small and the void works partially as a focusing element. It is known[26] that the focal length for such an element $f = R/2\delta = 67$ cm ($\delta = 2.61 \cdot 10^{-6}$) for considered parameters.

The focusing can explain the existence of black area and the narrow white area in the center of calculated map. On the other hand, the focusing phenomenon takes place for a refraction element (large object) which makes a huge maximum phase shift $p = K\delta t_0$. Here it is not the case because $p = 1.48$ therefore our object is mainly diffraction element. For example, for $R = 5$ cm the calculated image has the white area of smaller size while the focal length becomes larger.

The existence of interference fringes is also due to a diffraction nature of scattering. We note that the picture does not show very small interference fringes due to poor resolution of the image, but they are seen in the original calculated image. Such fringes cannot be resolved by modern CCD detectors with an optical magnification. We note as well that the synchrotron radiation is partially coherent due to a finite size of the source. The Pohang Light Source has a size of 60 $\mu$m vertically and 160 $\mu$m horizontally.

It is well known that a shift of point source on the distance $x_0$ from the optical axis leads to a shift of the picture as a whole at the detector on the distance $x_d = x_0 z_1/z_0$. Therefore for a comparison with the experiment the picture obtained with the point source should be smoothed over the region 0.6 $\mu$m vertically and 1.6 $\mu$m horizontally. They are rather small values. The more crucial is the detector resolution. The effective pixel size of the experimental images is 0.45 $\mu$m, but the real detector resolution is larger.

The bottom panel of Figure 4 show the image which was obtained from the top panel image by means of convolution with the Gaussian having FWHM (full width at half maximum) 2 $\mu$m vertically and 4 $\mu$m horizontally. This image looks like the experimental image shown in the bottom panel of Figure 2. To obtain the image with the pink beam it is necessary to calculate the images for various energies and to make a summation of all images according to effective spectrum to one image. It is clear that such a procedure makes the contrast of the image to be weaker.

However, as follows from Figure 2, use of a monochromated beam does not reveal fine peculiarities of the image which can be calculated with a fully coherent beam. The main reason is the

All article content, except where otherwise noted, is licensed under a Creative Commons Attribution 3.0 Unported license. See: http://creativecommons.org/licenses/by/3.0/
Downloaded to IP: 37.144.188.193 On: Wed, 24 Sep 2014 11:09:02

insufficient detector resolution. Although the image shows more contrast the exposure time increases crucially.

In conclusion, using computer simulation of phase contrast images we determined the shape and the size of capsule-like micro-voids in the crystalline wafer of 6*H*-SiC. The (0001) wafer was cut out from the boule grown on the $(11\bar{2}0)$ plane seed with a regularly grooved surface. High-flux multilayer monochromator could not reveal the fine features visible on calculated (fully coherent) images. Therefore a usage of the monochromator provides poor advantages compared with a pink beam. At the same time, the simulated images were in a good agreement with the experimental ones. Despite a finite detector resolution and a limited spatial coherence, we successfully reproduced the micro-void parameters. The images measured in the far field differ from the objects themselves, and to understand a void nature one has to perform the computer simulation.

The voids could form into a grown SiC crystal because of the grooves made on $(11\bar{2}0)$ surface of the seed which, in contrast to those on (0001) surface, failed to flatten. The vacancies were able to appear at the faces of the grooves, and their migration occurred quite easily. Suggestively, a strong temperature gradient made the voids obtain an elongated shape. The conditions for the capsule-like voids to develop into other types of voids, e.g., faceted or tubular ones, need further study.

## ACKNOWLEDGMENTS

The work of JHJ was supported by the Creative Research Initiatives (Functional x-ray Imaging) of MEST/NRF. The work of VGK was partially supported by RFBR grant N.13-02-00469 and by The Ministry of education and science of Russian Federation, project 8364.

[1] St. G. Müller, E. K. Sanchez, D. M. Hansen, R. D. Drachev, G. Chung, B. Thomas, J. Zhang, M. J. Loboda, M. Dudley, H. Wang, F. Wu, S. Byrappa, B. Raghothamachar, and G. Choi, J. Cryst. Growth **352**, 39 (2012).
[2] S. A. Sakwe, M. Stockmeier, P. Hens, R. Müller, D. Queren, U. Kunecke, K. Konias, R. Hock, A. Magerl, M. Pons, A. Winnacker, and P. Wellmann, Phys. Stat. Sol. (b) **245**, 1239 (2008).
[3] M. Dudley, X. R. Huang, W. Huang, A. Powell, S. Wang, P. Neudeck, and M. Skowronski, Appl. Phys. Lett. **75**, 784 (1999).
[4] J. Heindl, H. P. Strunk, V. D. Heydemann, and G. Pensl, Phys. Stat. Sol. (a) **162**, 251 (1997).
[5] T. A. Kuhr, E. K. Sanchez, M. Skowronski, W. M. Vetter, and M. Dudley, J. Appl. Phys. **89**, 4625 (2001).
[6] T. S. Argunova, M. Yu. Gutkin, J. H. Je, E. N. Mokhov, S. S. Nagalyuk, and Y. Hwu, Phys. Stat. Sol. (a) **208**, 819 (2011).
[7] V. G. Kohn, T. S. Argunova, and J. H. Je, Appl. Phys. Lett. **91**, 171901 (2007).
[8] M. Yu. Gutkin, A. G. Sheinerman, M. A. Smirnov, V. G. Kohn, T. S. Argunova, J. H. Je, and J. W. Jung, Appl. Phys. Lett. **93**, 151905 (2008).
[9] T. S. Argunova, V. G. Kohn, and J. H. Je, J. Surface Investig. **2**, 861 (2008).
[10] T. S. Argunova, V. G. Kohn, J. W. Jung, and J. H. Je, Phys. Stat. Solidi (a) **206**, 1833 (2009).
[11] V. G. Kohn, T. S. Argunova, and J. H. Je, J. Phys. D: Appl. Phys. **43**, 442002 (2010).
[12] V. G. Kohn, T. C. Argunova, and J. H. Je, J. Surface Investig. **5**, 1 (2011).
[13] M. Yu. Gutkin, A. G. Sheinerman, V. G. Kohn, T. S. Argunova, M. A. Smirnov, and J. H. Je, Phys. Stat. Sol. (a) **209**, 1432 (2012).
[14] V. G. Kohn, T. S. Argunova, and J. H. Je, J. Surface Investig. **6**, 840 (2012).
[15] V. G. Kohn, T. S. Argunova, and J. H. Je, AIP Advances **3**, 122109 (2013).
[16] P. Cloetens, M. Pateyron-Salomé, J. Y. Buffiére, G. Peix, J. Baruchel, F. Peyrin, and M. Schlenker, J. Appl. Phys. **81**, 5878 (1997).
[17] P. Cloetens, W. Ludwig, J. Baruchel, J.-P. Guigay, P. Pernot-Rejmánková, M. Salomé-Pateyron, M. Schlenker, J.-Y. Buffiére, E. Maire, and G. Peix, J. Phys. D: Appl. Phys. **32**, A145 (1999).
[18] A. Rack, S. Zabler, B. R. Müller, H. Riesemeier, G. Weidemann, A. Lange, J. Goebbels, M. Hentschel, and W. Görnerb, Nucl. Instrum. Methods Phys. Res., A **586**, 327 (2008).
[19] S. Zabler, T. Rack, A. Rack, and K. Nelson, Rev. Sci. Instrum. **81**, 103703 (2010).
[20] N. Ohtani, M. Katsuno, and T. Fujimoto, Jpn. J. Appl. Phys. **42**, L277 (2003).
[21] P. G. Neudeck, H. Du, M. Skowronski, D. J. Spry, and A. J. Trunek, J. Phys. D: Appl. Phys. **40**, 6139 (2007).
[22] E. N. Mokhov and S. S. Nagalyuk, Tech. Phys. Lett. **37**, 999 (2011).
[23] Yu. A. Vodakov, A. D. Roenkov, M. G. Ramm, E. N. Mokhov, and Yu. N. Makarov, Phys. Stat. Sol. (b) **202**, 177 (1997).
[24] A. Snigirev, I. Snigireva, V. Kohn, S. Kuznetsov, and I. Schelokov, Rev. Sci. Instrum. **66**, 5486 (1995).
[25] V. G. Kohn, J. Synchr. Rad. **19**, 84 (2012).
[26] A. Snigirev, V. Kohn, I. Snigireva, and B. Lengeler, Nature **384**, 49 (1996).

All article content, except where otherwise noted, is licensed under a Creative Commons Attribution 3.0 Unported license. See: http://creativecommons.org/licenses/by/3.0/
Downloaded to IP: 37.144.188.193 On: Wed, 24 Sep 2014 11:09:02